

## ORIGINAL PAPER

# Doping level of Mn in high temperature grown $Zn_{1-x}Mn_xO$ studied through electronic charge distribution, magnetization, and local structure

<sup>a</sup>Ramachandran Saravanan\*, <sup>a</sup>Santhanam Francis, <sup>b</sup>John L. Berchmans

<sup>a</sup>Research centre and PG Department of Physics, The Madura College, Madurai, 625 011, Tamil Nadu, India

<sup>b</sup>Electroprometallurgy division, CECRI, Karaikudi, 630 006, Tamil Nadu, India

Received 22 July 2011; Revised 21 November 2011; Accepted 21 November 2011

Mn inclusion in the oxide based diluted magnetic semiconductor  $Zn_{1-x}Mn_xO$  ( $x = 0.04, 0.06, 0.08, \text{ and } 0.10$ ) grown by standard high temperature solid state reaction technique has been studied. The local and average structure of  $Zn_{1-x}Mn_xO$  was characterized by the super resolution technique maximum entropy method and pair distribution function analysis using the X-ray powder data. Magnetic studies on this material using a Vibrating Sample Magnetometer were also carried out to ascertain the doping level in  $Zn_{1-x}Mn_xO$ .

© 2011 Institute of Chemistry, Slovak Academy of Sciences

## Introduction

For a long time, the spin of the electron has been ignored in the field of conventional electronics. Spintronics is a newly emerging field in solid state physics and information technology. Therefore, searching for new materials has become crucial from the viewpoints of both fundamental research and practical applications. Diluted magnetic semiconductors (DMS) are one of the most promising candidates for spintronics application. Currently, there is high scientific interest in the development of ZnO based dilute magnetic semiconductors (DMS) because they are used in spintronic devices such as spin-based sensors, light-emitters, transistors, etc. Magnetic behavior of such materials is caused by the introduction of transition metal (TM) ions, such as Mn, Co, Fe, and Cr, in appropriate concentrations in the host material. Spintronic devices have many advantages over semiconductor devices as higher speed, higher efficiency, and better stability. The field of spintronics is based on certain fundamental ideas of spin injection, scattering, transport, and detection. These phenomena have been applied to modern electronic devices. Advantages of these new devices are non-volatility, increased data

processing speed, low electronic power consumption, and increased integration densities compared to conventional semiconductor devices. Availability of such systems will enable the fabrication of the essential device elements required for a fully developed spintronics technology.

Recently, a number of research groups have reported ferromagnetism (FM) at room temperature in wide band gap materials (Sharma et al., 2003, 2007; Chen et al., 2005; Rubi et al., 2007; Pearton et al., 2003b). Room temperature FM was observed by Sharma et al. (2003) in bulk Mn doped ZnO. Chen et al. (2005) reported FM in samples treated in Ar atmosphere and the disappearance of FM in samples annealed in air. Ruby et al. (2007) reported that firing Mn doped ZnO in oxygen and Co doped ZnO in nitrogen atmosphere lead to FM interactions. Sharma et al. (2007) claim that the observed FM interactions in Mn doped ZnO are primarily due to the substitution of Mn ions at regular lattice sites of Zn.

Pearton et al. (2003b) showed that practical FM wide band gap DMS materials for spintronic applications require both the lattice site introduction of Mn as well as the careful control of the background defect concentration for the optimization of these ma-

\*Corresponding author, e-mail: saragow@dataone.in

terials. Pearton et al. (2003a) also discussed that the mechanism of the observed magnetic behavior is complicated and depends on a number of factors such as distance between  $\text{Mn}^{2+}$ – $\text{Mn}^{2+}$  ions, density of charge carriers, etc. Yan et al. (2007) reported room temperature FM in Mn doped ZnO. They proved that Mn atoms are substituted at the Zn sites, by Mn K-edge XAFS (X-ray absorption fine structure) studies. In addition, they found numerous Zn vacancies using the O-edge XAFS studies. Based on the first principles calculations, they predicted that Zn vacancy can induce room temperature FM in Mn doped ZnO. This super exchange mechanism can be viewed as an indirect exchange interaction mediated by the anions, thus involving the valence band (Norton et al., 2003). There is an explanation of FM in DMS materials given by the RKKY (Ruderman–Kittel–Kasuya–Yosida) theory (Priour et al., 2004). It has been predicted that magnetic properties in DMS materials are due to the interaction of polarized local electrons and conducting electrons. The increasing number of free charge carriers enhances the magnetic properties.

It seems that many contrasting results concerning magnetic properties in Mn doped ZnO are being obtained. From these reports it is obvious that the material processing parameters are important for the achievement of the desired magnetic properties. Tailoring of the free carriers' concentration depends

on the sample preparation conditions which involve a large number of parameters to control.

In this work, oxide based DMS material  $\text{Zn}_{1-x}\text{Mn}_x\text{O}$  ( $x = 0.04, 0.06, 0.08, \text{ and } 0.10$ ) has been studied to ascertain the level of Mn doping through the electronic structure, local distortion, optical band gap and magnetic behavior. The title compound was grown by a standard solid state reaction technique. The powder X-ray data sets were analyzed using the Rietveld method (Rietveld, 1969). To understand the distribution of charges in the host material with respect to Mn doping, the maximum entropy method (MEM) was used. Local structure of the material was analyzed using the pair distribution function (PDF) and the magnetic behavior using a vibrating sample magnetometer.

In this work, clear understanding in terms of structural, electronic, and magnetic properties of  $\text{Zn}_{1-x}\text{Mn}_x\text{O}$  and the doping level of Mn achieved using the high temperature solid state reaction method is gained. As already mentioned in the initial part of the introduction, physical, magnetic and optical properties of Mn doped ZnO depend on the transition metal (TM) ion Mn concentration in the host lattice.

## Experimental

$\text{Zn}_{1-x}\text{Mn}_x\text{O}$  ( $x = 0.04, 0.06, 0.08, \text{ and } 0.10$ ) sam-

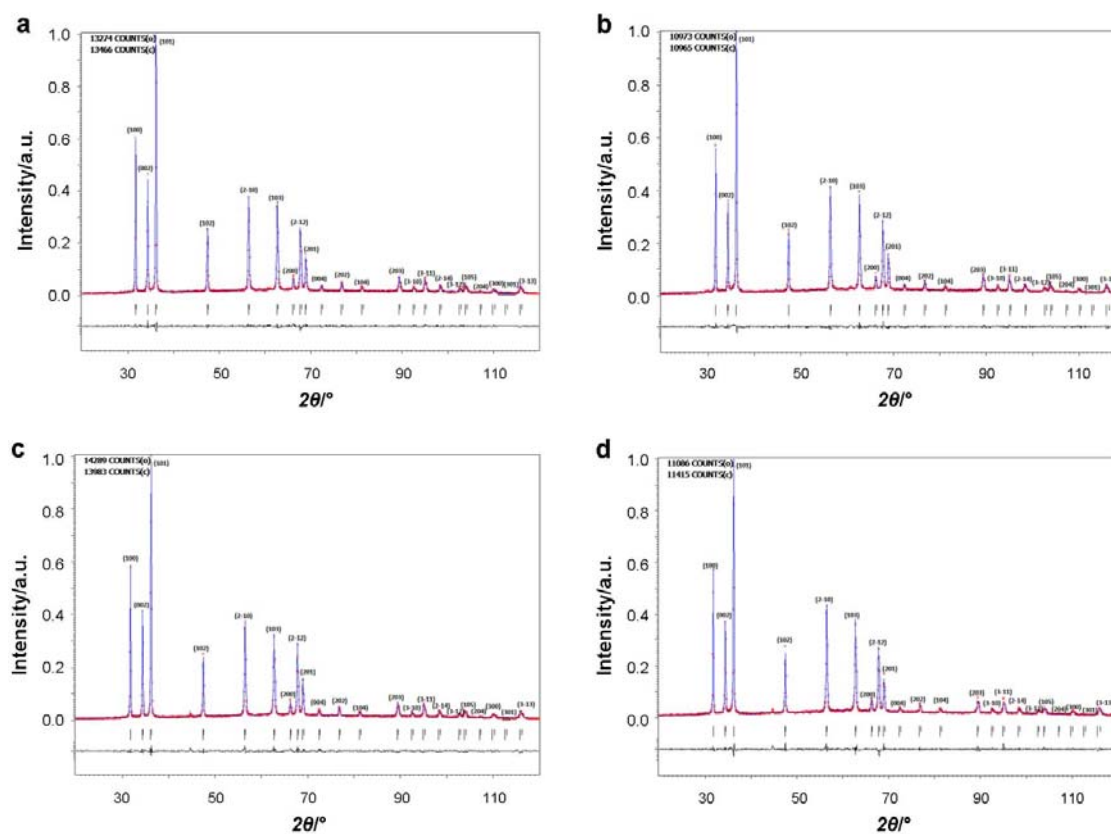


Fig. 1. Rietveld refined profiles for  $\text{Zn}_{1-x}\text{Mn}_x\text{O}$ ;  $x = 0.04$  (a),  $x = 0.06$  (b),  $x = 0.08$  (c),  $x = 0.10$  (d).

**Table 1.** Structural parameters of  $\text{Zn}_{1-x}\text{Mn}_x\text{O}$  from the Rietveld refinement

Parameter	$x$			
	0.04	0.06	0.08	0.10
$a/\text{Å}$	3.2637(1)	3.2696(4)	3.2779(6)	3.2849(8)
$c/\text{Å}$	5.2268(1)	5.2352(6)	5.2485(7)	5.2559(10)
$B_{\text{Zn}}/\text{Å}^2$	2.644(19)	2.612(27)	2.605(31)	2.551(27)
$B_{\text{O}}/\text{Å}^2$	2.061(12)	2.221(91)	2.487(133)	2.580(11)
$z/\text{O}$	0.8845(4)	0.8771(4)	0.8778 (07)	0.8706(02)
$R_{\text{obs}}/\%$	1.74	1.29	0.90	0.93
$wR_{\text{obs}}/\%$	2.27	1.85	1.41	1.29
$R_{\text{p}}/\%$	4.96	4.51	5.64	5.25
$wR_{\text{p}}/\%$	6.78	6.01	7.69	7.07

ples were grown by the standard high temperature solid state reaction technique. The high quality samples of ZnO (99.99 %, Otto Kemi, Mumbai, India) and  $\text{MnO}_2$  (99.98 %, Loba Chemie, Mumbai, India) were mixed in stoichiometric ratio and ground into fine powders using an agate mortar pestle for five hours. Mixed powders were carefully transferred to thick walled quartz ampoules. The ampoules were kept inside a vertical furnace (System control, Digital electrical resistance furnace, Chennai, India) at a final temperature of 1250 °C. Temperature inside the chamber was increased from ambient temperature to 700 °C in steps of 50 °C  $\text{h}^{-1}$ . From 700 °C, the temperature was increased in steps of 25 °C  $\text{h}^{-1}$  until 1000 °C. At this time, the samples were left soaking for 72 h and then the temperature was increased at the rate of 10 °C  $\text{h}^{-1}$  up to 1250 °C. The samples were then cooled slowly down at the rate of 50 °C  $\text{h}^{-1}$ . The synthesized powders were ground and pressed into pellets of 2 cm in diameter. The above procedure was repeated with the pellets to get single phase  $\text{Zn}_{1-x}\text{Mn}_x\text{O}$  samples.

The synthesized samples were characterized by powder X-ray ( $\text{CuK}\alpha$ ) diffraction analysis (Philips, X-PERT PRO, The Netherlands). The wavelength used for X-ray intensity data collection was 1.54056 Å. The  $2\theta$  range of data collection was 20–120° for all data sets with the step size of 0.05° in  $2\theta$ . These data sets were analyzed using the Rietveld (1969) profile fitting software JANA 2006 (Petříček et al., 2006). The fitted profiles are shown in Figs. 1a to 1d for  $x = 0.04, 0.06, 0.08,$  and  $0.10,$  respectively. Structural parameters of the refinements are given in Table 1.

Magnetic hysteresis curves were studied for the grown powder materials using a vibrating sample magnetometer (VSM) (Lakeshore International Corporation, 7404 SPEC, Westerville, USA) at room temperature. This instrument can measure magnetic moments in the range of  $10^{-7}$ – $10^3$  emu. The magnetic hysteresis curves were drawn between the field ( $G$ ) and the moment ( $\text{emu g}^{-1}$ ) and for  $\text{Zn}_{1-x}\text{Mn}_x\text{O}$  ( $x = 0.04, 0.06, 0.08,$  and  $0.10$ ) they are shown in Figs. 2a and 2b. Values of the saturation magnetization are given in Table 2.

**Table 2.** Saturation magnetization of  $\text{Zn}_{1-x}\text{Mn}_x\text{O}$  from VSM measurements

$x$	$10^3 \cdot M_{\text{s}}$	Difference in $10^3 \cdot M_{\text{s}}$ between successive values
		$\text{emu g}^{-1}$
0.04	0.047	–
0.06	0.054	0.007
0.08	0.084	0.030
0.10	0.099	0.015

**Table 3.** Band gap of  $\text{Zn}_{1-x}\text{Mn}_x\text{O}$  from UV-VIS studies

$x$	Band gap, $E_{\text{g}}$
	eV
0.00	3.20 <sup>a</sup>
0.00	3.35 <sup>b</sup>
0.04	3.70
0.06	2.80
0.08	2.90
0.10	3.45

a) Pearton et al. (2004), b) Norton et al. (2003)

Optical absorption spectra of  $\text{Zn}_{1-x}\text{Mn}_x\text{O}$  were recorded in the UV-VIS wavelength range of 2000–10000 Å (Thermo Scientific Corporation, Thermo Fisher Helios, Colorado, USA). A plot of  $(\alpha h\nu)^2$  and the photon energy  $E$  for various concentrations of Mn doping is shown in Fig. 3, where  $\alpha$  is the absorption coefficient. Band gap values deduced from the absorption spectra are given in Table 3.

## Results and discussion

### Rietveld analysis

Introduction of the Rietveld (Rietveld, 1969) technique was a significant step forward in the diffraction

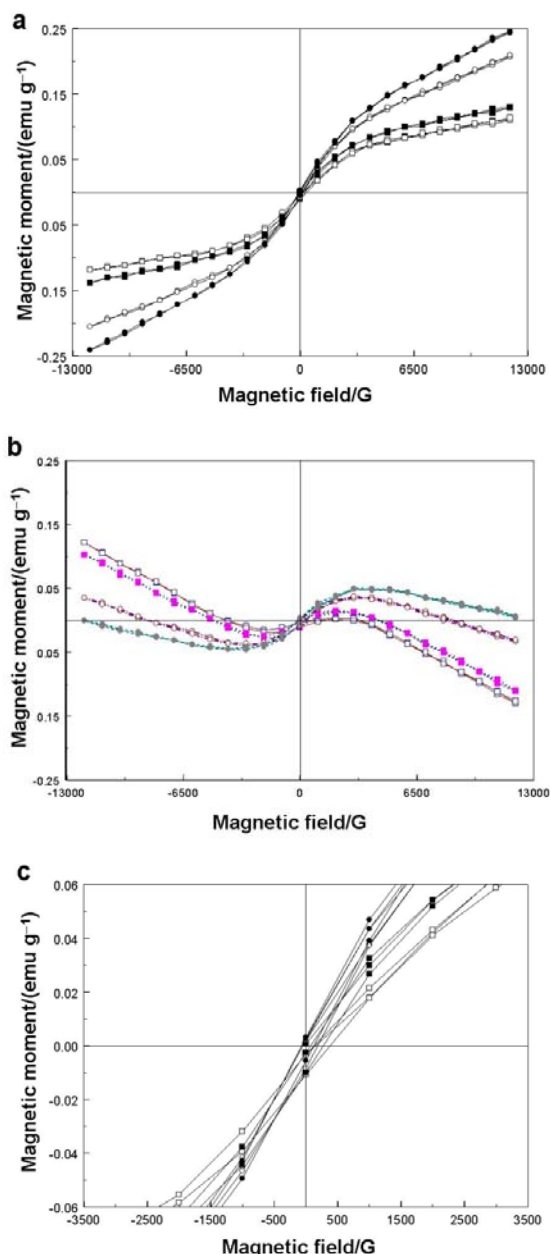


**Fig. 2.** Hysteresis loop at room temperature for  $\text{Zn}_{0.96}\text{Mn}_{0.04}\text{O}$  ( $\square$ ),  $\text{Zn}_{0.94}\text{Mn}_{0.06}\text{O}$  ( $\blacksquare$ ),  $\text{Zn}_{0.92}\text{Mn}_{0.08}\text{O}$  ( $\circ$ ), and  $\text{Zn}_{0.90}\text{Mn}_{0.10}\text{O}$  ( $\bullet$ ) (a). Ferromagnetic component of magnetization by subtraction of the linear paramagnetic component for  $\text{Zn}_{0.96}\text{Mn}_{0.04}\text{O}$  ( $\square$ ),  $\text{Zn}_{0.92}\text{Mn}_{0.08}\text{O}$  ( $\blacksquare$ ),  $\text{Zn}_{0.90}\text{Mn}_{0.10}\text{O}$  ( $\circ$ ), and  $\text{Zn}_{0.94}\text{Mn}_{0.06}\text{O}$  ( $\bullet$ ) (b). Close up view near  $H = 0$  Oe for  $\text{Zn}_{0.96}\text{Mn}_{0.04}\text{O}$  ( $\square$ ),  $\text{Zn}_{0.92}\text{Mn}_{0.08}\text{O}$  ( $\blacksquare$ ),  $\text{Zn}_{0.90}\text{Mn}_{0.10}\text{O}$  ( $\circ$ ), and  $\text{Zn}_{0.94}\text{Mn}_{0.06}\text{O}$  ( $\bullet$ ) (c).

analysis of powder samples. This refinement technique is more widely applicable for the characterization of crystalline materials. The Rietveld method uses the least squares approach to refine an observed profile until it matches the calculated profile. In the Rietveld refinement analysis, all the structural and profile parameters are refined to get accurate information on

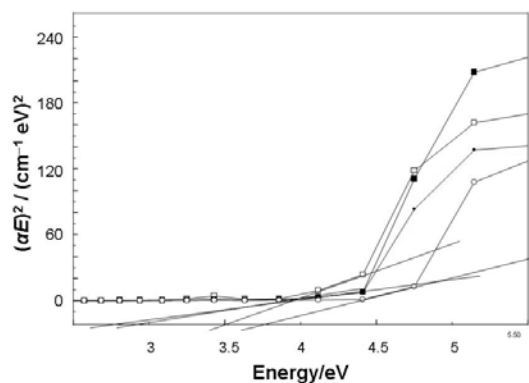


**Fig. 3.** UV-VIS spectra as a plot of  $(\alpha h\nu)^2$  vs. the photon energy.  $\text{Zn}_{0.96}\text{Mn}_{0.04}\text{O}$  ( $\circ$ ),  $\text{Zn}_{0.94}\text{Mn}_{0.06}\text{O}$  ( $\bullet$ ),  $\text{Zn}_{0.92}\text{Mn}_{0.06}\text{O}$  ( $\square$ ), and  $\text{Zn}_{0.90}\text{Mn}_{0.10}\text{O}$  ( $\blacksquare$ ).

the structure. It was performed for all the data sets of  $\text{Zn}_{1-x}\text{Mn}_x\text{O}$  using the software package JANA 2006 (Petříček et al., 2006). The lattice parameter, fractional atomic coordinates, atomic displacement parameters, and the occupation factors were obtained from whole powder diffraction patterns. Figs. 1a–1d show the refined profiles of crystalline  $\text{Zn}_{1-x}\text{Mn}_x\text{O}$  samples for the doping concentrations  $x = 0.04, 0.06, 0.08,$  and  $0.10,$  respectively, and the observed and calculated profiles match very well. In the refined profiles, Figs. 1c ( $x = 0.08$ ) and 1d ( $x = 0.10$ ) show a small additional peak appearing at around  $2\theta = 45^\circ$  due to the presence of the  $\text{ZnMn}_2\text{O}_4$  phase whose intensities and phase fraction are very low (the additional peak at around  $2\theta = 45^\circ$  corresponds to the most intense Bragg reflection (2 1 1) of  $\text{ZnMn}_2\text{O}_4$ ). The phase fraction of this compound could not be reliably refined.

It can also be found from Table 1 that the Debye–Waller factor  $B_{\text{iso}}$  values of the Zn(Mn) atom decrease with the Mn concentration and the  $B_{\text{iso}}$  values of the oxygen atom increase with the Mn doping. The addition of more Mn atoms in the host lattice leads to increased static distortion in the oxygen atom through the Zn(Mn)–O coupling, which is evident from the 3D electron density distributions shown in Figs. 4a–4d. Ionic radii of divalent  $\text{Zn}^{2+}$  and  $\text{Mn}^{2+}$  are  $0.60 \text{ \AA}$  and  $0.66 \text{ \AA}$ , respectively (Shannon, 1976). Hence, the addition of more  $\text{Mn}^{2+}$  cations in the lattice replacing  $\text{Zn}^{2+}$  leads to more mis-possession of  $\text{Zn}^{2+}$  from its regular lattice sites and to apparent Zn site vacancies in the lattice. From the MEM analysis it is clear that at  $x = 0.08$  and  $x = 0.10$ , inclusion of Mn at the interstitial positions also occurs, apart from regular host lattice positions of Zn. The mid-bond density between Zn and O ( $-x, -y, z + 0.5$ ) decreases at  $x = 0.08$  and then increases. This fact is probably due to the mis-possession of the Zn atom from its regular site. The increase in electron density at  $x = 0.10$  can be attributed to a higher number of Zn atoms at reg-

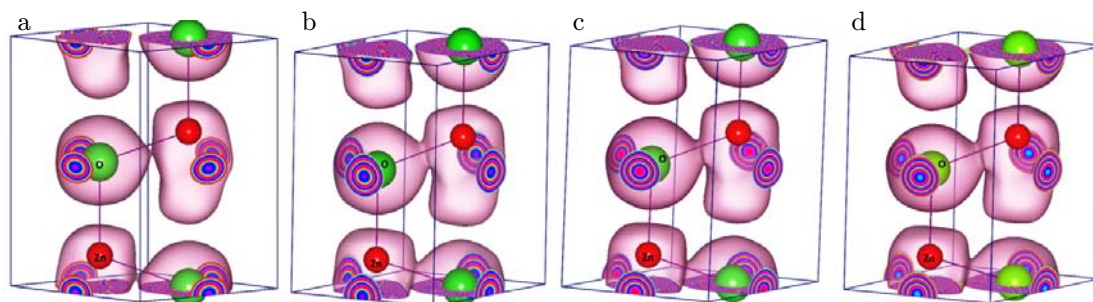


**Fig. 4.** Three dimensional charge density of  $Zn_{1-x}Mn_xO$  in the unit cell  $x = 0.04$  (a),  $x = 0.06$  (b),  $x = 0.08$  (c),  $x = 0.10$  (d).

**Table 4.** Parameters from the MEM analysis

Parameter	$x$			
	0.04	0.06	0.08	0.10
Number of cycles	122	115	120	122
Prior density, $\tau(\tau_1)/\text{\AA}^{-3}$	1.3688	1.3630	1.3612	1.3580
Lagrange parameter, $\lambda$	0.00560	0.00557	0.00559	0.00560
$R_{MEM}/\%$	1.133	1.184	1.160	1.164
$wR_{MEM}/\%$	1.359	1.410	1.392	1.400

ular and also at interstitial sites leading to enhanced charge density.

#### Charge distribution in $Zn_{1-x}Mn_xO$

In this work, electronic structure of  $Zn_{1-x}Mn_xO$  was analyzed by the maximum entropy method (MEM) using the structure factors obtained from X-ray measurements. The MEM calculations (Izumi & Dilanian, 2002) were carried out for all the datasets of  $Zn_{1-x}Mn_xO$ . The MEM electron densities compiled from the experimental information were used for the visualization of the 3D electron density using the software VESTA (Momma & Izumi, 2008). The charge densities of  $Zn_{1-x}Mn_xO$  in the unit cell can be clearly seen from the three dimensional iso-surfaces shown in Figs. 4a–4d. Enhanced spatial distribution of charges for the oxygen atom compared to the Zn(Mn) atom can be seen. As the Mn concentration increases the charge distribution between the Zn and O atoms situated at  $(-x, -y, z + 0.5)$  increases. But the trend is not as it should be when Mn concentration increases, i.e., the enhancement of charge clouds between the Zn and O atoms could not be visualized unambiguously. Hence, it is clear that despite the inclusion of Mn atoms in the host lattice Zn, there is additional segregation of Mn atoms probably at interstitial positions, which leads to the decreased charge distribution at the Zn atomic sites. The parameters involved in this analysis are presented in Table 4. In the present work, computation of the charge density was done using the software PRIMA (Izumi & Dilanian, 2002) employing the maximum entropy method (MEM) tech-

nique and the resultant density was plotted with the help of the visualization software VESTA (Momma & Izumi, 2008). The refined structure factors were used for the electron density mapping by MEM (maximum entropy method). The space group of these systems was taken to be P63mc. The MEM electron density studies were carried out as mentioned in some research papers published by one of the authors (Saravanan & Prema Rani, 2007; Saravanan et al., 2007, 2008).

The study of electron densities was carried out as 3D, 2D, and 1D analyses. Figs. 5a–5d show the two dimensional electron density distributions for  $Zn_{0.96}Mn_{0.04}O$ ,  $Zn_{0.94}Mn_{0.06}O$ ,  $Zn_{0.92}Mn_{0.08}O$ , and  $Zn_{0.90}Mn_{0.10}O$  on the (110) plane. Careful examination of these figures shows expansion of both the Zn(Mn) and the O atoms with the increase of the Mn concentration, though it is steeper for the oxygen atom. In the 2D contour maps, also the expansion of the charge clouds could not be seen clearly, indicating the interstitial addition of Mn atoms. The MEM electron densities along two different Zn(Mn)—O bonding directions are shown in Table 5. In both types of bonding (covalent and ionic), there is in general, an increase in the electron densities with the increasing Mn concentration though slight variations are found in both cases, which can be accounted for by the interstitial additions of Mn atoms. The one dimensional electron density profiles of  $Zn_{1-x}Mn_xO$  drawn along the two different directions (Zn—O at  $-x, -y, z + 1/2$ ; and Zn—O at  $-y, x - y, z$ ) corresponding to Zn—O bonds are shown in Fig. 6. Fig. 6a shows the covalent type interactions in the Zn(Mn)—O bond and Fig. 6b shows the ionic nature of this bond.

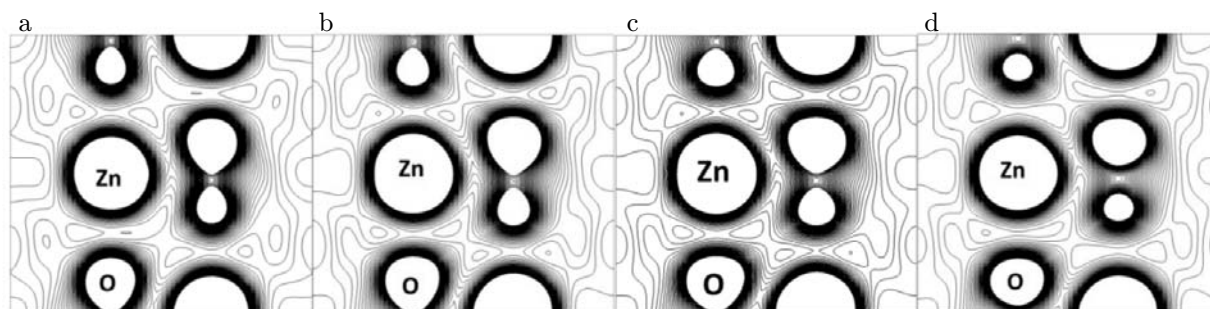


**Fig. 5.** 2D MEM electron density distribution of  $\text{Zn}_{1-x}\text{Mn}_x\text{O}$  on the (110) plane.  $x = 0.04$  (a),  $x = 0.06$  (b),  $x = 0.08$  (c),  $x = 0.10$  (d). Contour range:  $0.00\text{--}2.00 \text{ \AA}^{-3}$ , contour interval:  $0.03 \text{ \AA}^{-3}$ .

**Table 5.** MEM electron density of  $\text{Zn}_{1-x}\text{Mn}_x\text{O}$  in the Zn(Mn)—O bond

$x$	Zn—O ( $-x, -y, z + 1/2$ ), covalent type		Zn—O ( $-y, x - y, z$ ), ionic type	
	Distance	Density	Distance	Density
	$\text{Å}$	$\text{Å}^{-3}$	$\text{Å}$	$\text{Å}^{-3}$
0.04	1.09	0.48	1.11	0.25
0.06	1.09	0.55	1.14	0.32
0.08	1.10	0.54	1.14	0.34
0.10	1.09	0.58	1.14	0.30

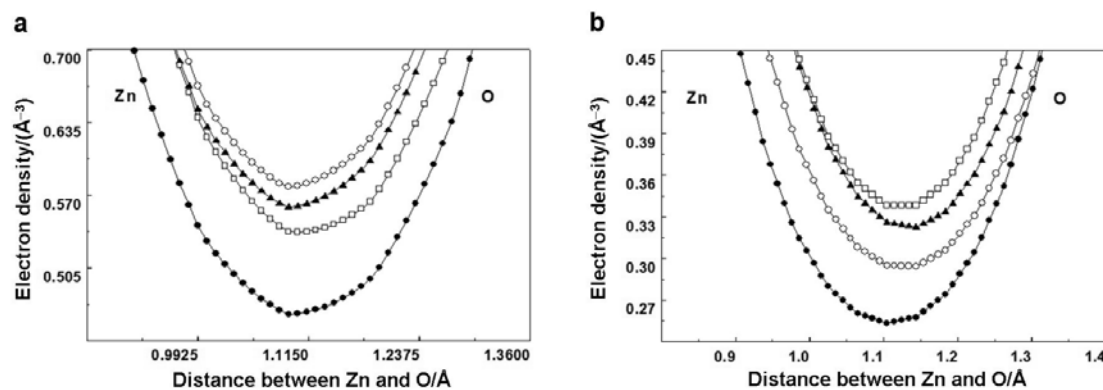


**Fig. 6.** 1D variation of electron density between Zn and O at ( $-x, -y, z + 1/2$ ):  $\text{Zn}_{0.96}\text{Mn}_{0.04}\text{O}$  (●),  $\text{Zn}_{0.94}\text{Mn}_{0.06}\text{O}$  (◄),  $\text{Zn}_{0.92}\text{Mn}_{0.08}\text{O}$  (◻), and  $\text{Zn}_{0.90}\text{Mn}_{0.10}\text{O}$  (○) (a). 1D variation of electron density between Zn and O at ( $-y, x - y, z$ ):  $\text{Zn}_{0.96}\text{Mn}_{0.04}\text{O}$  (●),  $\text{Zn}_{0.94}\text{Mn}_{0.06}\text{O}$  (bltriang),  $\text{Zn}_{0.92}\text{Mn}_{0.08}\text{O}$  (◻), and  $\text{Zn}_{0.90}\text{Mn}_{0.10}\text{O}$  (○).

### Local distortion in $\text{Zn}_{1-x}\text{Mn}_x\text{O}$

Different techniques for structure determination have been developed over the years. The pair distribution function (PDF) (Wagner, 1978; Warren, 1990; Egami, 1990) is widely used to study low order systems but it can be used also to study the structure of crystalline matter. The Rietveld type refinements (Rietveld, 1969) of powder data yield only an average structure since only Bragg intensities are used to deduce the structure. But the PDF is obtained through the Fourier transformation of the total scattering intensities including the Bragg and diffuse scattering components which can provide information on the local undulations in the structure (Egami, 1998).

The atomic pair distribution function can be obtained from the experimental powder diffraction data. In this work, the local disorder due to the doping of Mn in ZnO was analyzed using this technique. The pair distribution functions of  $\text{Zn}_{1-x}\text{Mn}_x\text{O}$  were obtained from the observed powder data sets using the software PDFgetx (Jeong et al., 2001). Then, observed PDF's were compared and refined using the software PDFgui (Farrow et al., 2007). The fitted PDF of  $\text{Zn}_{0.96}\text{Mn}_{0.04}\text{O}$  is given in Fig. 7a. Fig. 7b represents the observed PDF values of all the compositions of Mn, i.e.,  $x = 0.04, 0.06, 0.08,$  and  $0.10$ . It was found from Fig. 7b that the PDF values are in general in the decreasing order from  $x = 0.04$  to  $x = 0.10$  throughout the range  $r = 2\text{--}30 \text{ Å}$ . But undulations of this trend

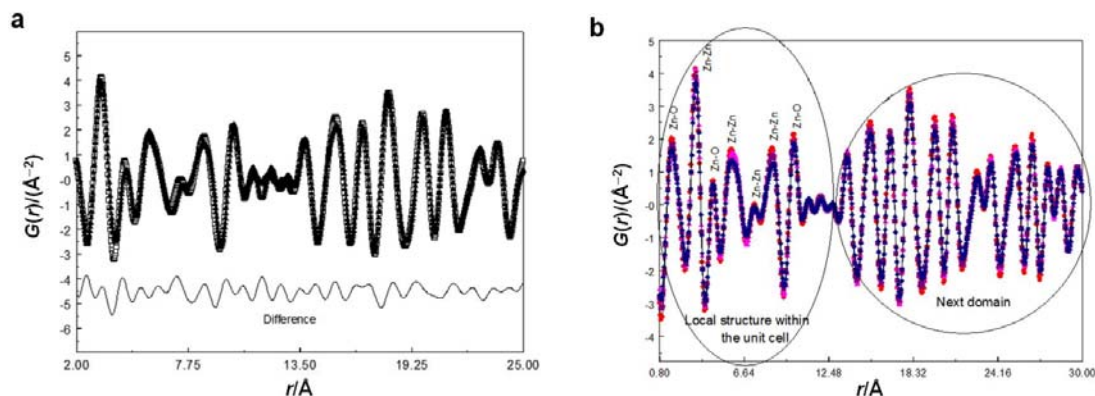


**Fig. 7.** Observed and calculated PDF of:  $\text{Zn}_{1-x}\text{Mn}_x\text{O}$  for  $x = 0.04$  (a),  $\text{Zn}_{1-x}\text{Mn}_x\text{O}$  for  $x = 0.04$ ,  $x = 0.06$ ,  $x = 0.08$ , and  $x = 0.10$ . The domain structure is visible (b). Domains represent the distribution of atomic neighbor distances and the number density of atoms.

can also be seen at various distances from 2 Å to 30 Å. These fluctuations in the trend indicate local fluctuations of the addition of Mn in the host lattice. Since, PDF gives the atomic number concentration and the atomic number of Mn is lower than that of Zn, addition of more and more Mn should lead to the decrease in the PDF value in which undulations occur, indicating an addition of Mn other than the host lattice. The observed bond lengths in general show an increased bond length distribution with respect to the concentration of Mn. The PDF values in Fig. 7b also show the domain structure of the unit cell and the variations of bond lengths in the domain. The PDF values from about the distance of 13 Å show the next domain and the local variations of number density and inter atomic distances in this domain. The capability of PDF procedure to analyze the domain structure has also been validated.

### Magnetic properties

In this work, to study the magnetic properties of the grown material, hysteresis curves were obtained using a vibrating sample magnetometer (VSM). Jeyakumar et al. (2006) reported that Mn doped ZnO showed mixed paramagnetic–ferromagnetic interactions. In this work, magnetic behavior of transition metal Mn doped ZnO bulk samples was studied at room temperature, because it is obvious that the growth conditions influence the magnetic properties of Mn doped ZnO. Curves of the magnetic field versus the magnetic moment shown in Fig. 2a prove that paramagnetic behavior increases with the Mn concentration. But ferromagnetic order is observed at all the concentrations studied. Hence, the paramagnetic component was subtracted from the total magnetization and the resultant hysteresis curves are shown in Fig. 2b. The close up view of Fig. 2a near  $H = 0$  Oe is shown in Fig. 2c. The slope of the hysteresis curves (Fig. 2a) and the saturation magnetization ( $M_s$ ) (Table 2) increase at the Mn addition, showing increased

paramagnetism in this material at the addition of Mn atoms.

It has been reported that Zn vacancies can induce room temperature ferromagnetism in Mn doped ZnO (Iusan et al., 2006). If the valence state of Mn is  $\text{Mn}^{3+}$  (ionic radius of  $\text{Mn}^{3+}$  is 0.58 Å (Shannon, 1976)), then, there is a possibility of Mn–Mn distances reduction which can lead to antiferromagnetic interactions (Iusan et al., 2006; Karamat et al., 2008). Our magnetic studies show clear paramagnetic behavior of all samples studied, the PM interactions being more intense in  $\text{Zn}_{0.90}\text{Mn}_{0.10}\text{O}$ . Hence, the valence state of most of the implanted Mn was proven to be  $\text{Mn}^{2+}$ ; these ions replace the host ions  $\text{Zn}^{2+}$  in the regular lattice sites. The observed magnetic behavior in our samples is due to the inclusion of  $\text{Mn}^{2+}$  ions in the regular lattice sites of  $\text{Zn}^{2+}$ . With the uniform increase of the Mn concentration, there should be a uniform increase in the paramagnetism as  $x$  values increase. Still, variations in this trend show that the observed difference in the saturation magnetization is not uniform with respect to the Mn concentration ( $x = 0.04$ , 0.06, 0.08, and 0.10). The difference in the  $M_s$  values between  $x = 0.06$  and  $x = 0.08$  is large, 0.002386 emu, indicating uneven addition of Mn in these compositions. The  $M_s$  values as evidenced from the hysteresis curves for  $x = 0.08$  and  $x = 0.10$  are much higher than those for  $x = 0.04$  and  $x = 0.06$ , indicating uneven doping of Mn at the interstitial positions at these two concentrations and additional magnetism due to the secondary phase  $\text{ZnMn}_2\text{O}_4$ .

### Band gap from optical absorption spectra

Energy of the incident photon ( $h\nu$ ) can be related to the band gap ( $E_g$ ) (Tauc et al., 1966; Pancove, 1979) through the following relation:

$$\alpha = \frac{A}{h\nu} (h\nu - E_g)^{\frac{m}{2}} \quad (1)$$

where  $m = 1$  for direct band gap materials and

$m = 4$  for indirect band gap materials,  $\alpha$  is the absorption coefficient,  $A$  is a constant,  $h$  is the Planck's constant,  $\nu$  is the frequency of the incident photon (Hz), and  $E_g$  is the band gap energy (eV). ZnO is a direct band gap material and hence:

$$(\alpha h\nu)^2 = A(h\nu - E_g) \quad (2)$$

The optical UV-VIS spectra, as shown in Fig. 3, reveal the increasing trend in the absorption with the increase of the Mn concentration. The value of the band gap decreases with the Mn concentration (Table 3) as deduced from the linear interpolation of the energy from the plot of  $(\alpha h\nu)^2$  and the photon energy  $E$  (Fig. 3). Reports are available on the reduction of the band gap on substitution of divalent metal atoms in ZnO. For example, Singh and Mohan (1975) reported a decrease in the band gap of ZnO at the addition of Co. Akyuz et al. (2006) and Yuonesi et al. (2008) reported the decrease in the band gap in ZnO at the addition of Mn at low concentrations of Mn. The increasing trend in electron densities (Table 5) with Mn doping is in line with the fact that the band gap decreases as shown in Table 3. Since, there is no phase change in the structure of  $\text{Zn}_{1-x}\text{Mn}_x\text{O}$  with the addition of Mn, the band gap decrease is observed in all the Mn concentrations studied in this work. However, from  $x = 0.06$ , undulations in the trend of the band gap can be observed, which results from uneven doping at concentrations starting at the value of 0.06. Shinde et al. (2006) observed a decrease in the transmittance and band gap energy at the addition of Mn in ZnO. Mn doped ZnO shows strong optical absorption with the threshold energy of about 2 eV as reported by Pearton et al. (2004). Our results on Mn doped ZnO show similar trends.

## Conclusions

The present investigations on Mn doped ZnO show an enhancement of paramagnetic behavior at the addition of Mn in the host lattice. Deviations in the magnetic and optical properties from the expected trend are attributed to the uneven dosing of Mn at the concentrations starting from  $x = 0.06$ . Ferromagnetic interactions are probably suppressed in the high temperature grown samples due to Mn–Mn antiferromagnetic interactions.

*Acknowledgements.* One of the authors (Dr. R. Saravanan) acknowledges the Council of Scientific and Industrial Research (CSIR) for financial assistance to the research project No.: 03(1138)/09/EMR-II.

## Symbols

$A$	constant	
$a$	cell parameter of unit cell	Å (nm)

$B_{\text{iso}}$	Debye–Waller factor	Å <sup>2</sup> (nm <sup>2</sup> )
$B_{\text{O}}$	Debye–Waller factor	Å <sup>2</sup> (nm <sup>2</sup> )
$B_{\text{Zn}}$	Debye–Waller factor	Å <sup>2</sup> (nm <sup>2</sup> )
$c$	cell parameter of unit cell	Å (nm)
$E$	photon energy	eV (J)
$E_g$	band gap energy	eV (J)
$G(r)$	atomic pair distribution function	Å <sup>-2</sup> (nm <sup>-2</sup> )
$H$	magnetic field	Oe (A m <sup>-1</sup> )
$M_s$	saturation magnetization	emu g <sup>-1</sup> (T)
$m$	constant	
$p_m$	magnetic moment	emu g <sup>-1</sup> (T)
$R_{\text{MEM}}$	MEM reliability index	%
$R_{\text{obs}}$	reliability index	%
$R_p$	profile reliability index	%
$r$	radial distance	Å (nm)
$wR_{\text{MEM}}$	weighted reliability index	%
$wR_{\text{obs}}$	weighted reliability index	%
$wR_p$	weighted profile reliability index	%
$z(\text{O})$	coordinate of the oxygen atom	
$\alpha$	absorption coefficient	
$\lambda$	Lagrange parameter	
$\nu$	frequency of incident photon	Hz
$\rho$	electron density	Å <sup>-3</sup> (nm <sup>-3</sup> )
$\tau(r_i)$	prior density	Å <sup>-3</sup> (nm <sup>-3</sup> )

## References

- Akyuz, I., Kose, S., Atay, F., & Bilgin, V. (2006). The optical, structural and morphological properties of ultrasonically sprayed ZnO:Mn films. *Semiconductor Science and Technology*, 21, 1620–1626. DOI: 10.1088/0268-1242/21/12/020.
- Chen, W., Zhao, L. F., Wang, Y. Q., Miao, J. H., Liu, S., Xia, Z. C., & Yuan, S. L. (2005). Effects of temperature and atmosphere on the magnetism properties of Mn-doped ZnO. *Applied Physics Letters*, 87, 42507. DOI: 10.1063/1.1952570.
- Egami, T. (1990). Atomic correlations in non-periodic matter. *Materials Transactions, JIM*, 31, 163–176.
- Egami, T. (1998). PDF analysis applied to crystalline materials. In S. J. L. Billinge, & M. F. Thorpe (Eds.), *Local structure from diffraction*. New York, NY, USA: Plenum Press. DOI: 10.1007/0-306-47077-2.1.
- Farrow, C. L., Juhas, P., Liu, J. W., Bryndin, D., Božin, E. S., Bloch, J., Proffen, Th., & Billinge, S. J. L. (2007). PDFfit2 and PDFgui: computer programs for studying nanostructure in crystals. *Journal of Physics: Condensed Matter*, 19, 335219. DOI: 10.1088/0953-8984/19/33/335219.
- Iusan, D., Sanyal, B., & Eriksson, O. (2006). Theoretical study of the magnetism of Mn-doped ZnO with and without defects. *Physical Review B*, 74, 235208. DOI: 10.1103/PhysRevB.74.235208.
- Izumi, F., & Dilanian, R. A. (2002). *Recent research developments in physics* (Vol. 3, Part II, pp. 699–726). Trivandrum, Kerala, India: Transworld Research Network.
- Jayakumar, O. D., Salunke, H. G., Kadam, R. M., Mohapatra, M., Yaswant, G., & Kulshreshtha, S. K. (2006). Magnetism in Mn-doped ZnO nanoparticles prepared by a co-precipitation method. *Nanotechnology*, 17, 1278–1285. DOI: 10.1088/0957-4484/17/5/020.
- Jeong, I. K., Thompson, J., Proffen, Th., Turner, A. M. P., & Billinge, S. J. L. (2001). *PDFgetX*: a program for obtaining the atomic pair distribution function from X-ray powder diffraction data. *Journal of Applied Crystallography*, 34, 536. DOI: 10.1107/s0021889801011487.

- Karamat, S., Mahmood, S., Lin, J. J., Pan, Z. Y., Lee, P., Tan, T. L., Springham, S. V., Ramanujan, R. V., & Rawat, R. S. (2008). Structural, optical and magnetic properties of  $(\text{ZnO})_{1-x}(\text{MnO}_2)_x$  thin films deposited at room temperature. *Applied Surface Science*, 254, 7285–7289. DOI: 10.1016/j.apsusc.2008.05.318.
- Momma, K., & Izumi, F. J. (2008). VESTA: a three-dimensional visualization system for electronic and structural analysis. *Journal of Applied Crystallography*, 41, 653–658. DOI: 10.1107/s0021889808012016.
- Norton, D. P., Pearton, S. J., Hebard, A. F., Theodoropoulou, N., Boatner, L. A., & Wilson, R. G. (2003). Ferromagnetism in Mn-implanted ZnO:Sn single crystals. *Applied Physics Letters*, 82, 239–241. DOI: 10.1063/1.1537457.
- Pancove, J. (1979). *Optical processes in semiconductors*. Englewood Cliffs, NJ, USA: Prentice-Hall.
- Pearton, S. J., Abernathy, C. R., Overberg, M. E., Thaler, G. T., Norton, D. P., Theodoropoulou, N., Hebard, A. F., Park, Y. D., Ren, F., Kim, J., & Boatner, L. A. (2003a). Wide band gap ferromagnetic semiconductors and oxides. *Journal of Applied Physics*, 93, 1–13. DOI: 10.1063/1.1517164.
- Pearton, S. J., Abernathy, C. R., Thaler, G. T., Frazier, R., Ren, F., Hebard, A. F., Park, Y. D., Norton, D. P., Tang, W., Stavola, M., Zavada, J. M., & Wilson, R. G. (2003b). Effects of defects and doping on wide band gap ferromagnetic semiconductors. *Physica B: Condensed Matter*, 340–342, 39–47. DOI: 10.1016/j.physb.2003.09.003.
- Pearton, S. J., Norton, D. P., Ip, K., Heo, Y. W., & Steiner, T. (2004). Recent advances in processing of ZnO. *Journal of Vacuum Science and Technology B*, 22, 932–948. DOI: 10.1116/1.1714985.
- Petríček, V., Dušek, M., & Palatinus, L. (2006). JANA 2006. The crystallographic computing system [computer software]. Prague, Czech Republic: Academy of Sciences of the Czech Republic.
- Priour, D. J., Hwang, E. H., & Das Sarma, S. (2004). Disordered RKKY lattice mean field theory for ferromagnetism in diluted magnetic semiconductors. *Physics Review Letters*, 92, 117201. DOI: 10.1103/PhysRevLett.92.117201.
- Rietveld, H. M., (1969). A profile refinement method for nuclear and magnetic structures. *Journal of Applied Crystallography*, 2, 65–71. DOI: 10.1107/s0021889869006558.
- Rubi, D., Fontcuberta, J., Calleja, A., Aragonès, Ll., Capdevila, X. G., & Segarra, M. (2007). Reversible ferromagnetic switching in ZnO:(Co, Mn) powders. *Physical Review B*, 75, 155322. DOI: 10.1103/physRevB.75.155322.
- Saravanan, R., Majella Mary Ann, A., & Jainulabdeen, S. (2007). Non-nuclear maxima (NNM), symmetric and asymmetric charge distribution in solar grade Si and n-GaAs, using X-ray powder data. *Physica B: Condensed Matter*, 400, 16–21. DOI: 10.1016/j.physb.2007.06.010.
- Saravanan, R., & Prema Rani, M. (2007). Maximum entropy method and multipole analysis of the bonding in sodium and vanadium metals. *Journal of Physics: Condensed Matter*, 19, 266221. DOI: 10.1088/0953-8984/19/26/266221.
- Saravanan, R., Syed Ali, K. S., & Israel, S. (2008). Electron density distribution in Si and Ge using multipole, maximum entropy method and pair distribution function analysis. *Pramana-Journal of Physics*, 70, 679–696. DOI: 10.1007/s12043-008-0029-9.
- Shannon, R. D. (1976). Revised effective ionic radii and systematic studies of interatomic distances in halides and chalcogenides. *Acta Crystallographica Section A*, 32, 751–767. DOI: 10.1107/s0567739476001551.
- Sharma, P., Gupta, A., Rao, K. V., Owens, F. J., Sharma, R., Ahuja, R., Osorio Guillen, J. M., Johansson, B., & Gehring, G. A. (2003). Ferromagnetism above room temperature in bulk and transparent thin films of Mn-doped ZnO. *Nature Materials*, 2, 673–677. DOI: 10.1038/nmat984.
- Sharma, V. K., Xalxo, R., & Varma, G. D. (2007). Structural and magnetic studies of Mn-doped ZnO. *Crystal Research and Technology*, 42, 34–38. DOI: 10.1002/crat.200610766.
- Shinde, V. R., Gujar, T. P., Lokhande, C. D., Mane, R. S., & Han, S. H. (2006). Mn doped and undoped ZnO films: A comparative structural, optical and electrical properties study. *Materials Chemistry and Physics*, 96, 326–330. DOI: 10.1016/j.matchemphys.2005.07.045.
- Singh, L. K., & Mohan, H. (1975). Optical semiconductor element and fabricating method. *Indian Journal of Pure & Applied Physics*, 13, 486–488.
- Tauc, J., Grigorovici, R., & Vancu, A. (1966). Optical properties and electronic structure of amorphous germanium. *Physica Status Solidi (b)*, 15, 627–637. DOI: 10.1002/pssb.19660150224.
- Wagner, C. N. J. (1978). Direct methods for the determination of atomic-scale structure of amorphous solids (X-ray, electron, and neutron scattering). *Journal of Non-Crystalline Solids*, 31, 1–40. DOI: 10.1016/0022-3093(78)90097-2.
- Warren, B. E. (1990). *X-ray diffraction*. New York, NY, USA: Dover Books on Physics.
- Yan, W., Sun, Z., Liu, Q., Li, Z., Pan, Z., Wang, J., Wei, S., Wang, D., Zhou, Y., & Zhang, X. (2007). Zn vacancy induced room-temperature ferromagnetism in Mn-doped ZnO. *Applied Physics Letters*, 91, 062113. DOI: 10.1063/1.2769391.
- Yuonesi, M., Ghazi, M. E., Izadifard, M., & Yaghobi, M. (2008). The optical and structural properties of ZnO:Mn nano films grown by sol-gel. *Journal of Optoelectronics and Advanced Materials*, 10, 2603–2606.